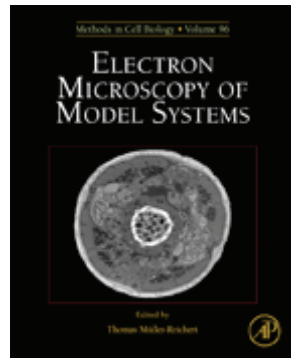


**Provided for non-commercial research and educational use only.  
Not for reproduction, distribution or commercial use.**

This chapter was originally published in the book *Methods in Cell Biology (Volume 96)*. The copy attached is provided by Elsevier for the author's benefit and for the benefit of the author's institution, for non-commercial research, and educational use. This includes without limitation use in instruction at your institution, distribution to specific colleagues, and providing a copy to your institution's administrator.



All other uses, reproduction and distribution, including without limitation commercial reprints, selling or licensing copies or access, or posting on open internet sites, your personal or institution's website or repository, are prohibited. For exceptions, permission may be sought for such use through Elsevier's permissions site at:

<http://www.elsevier.com/locate/permissionusematerial>

From Thomas H. Giddings, Electron Tomography and Immuno-labeling of  
Tetrahymena thermophila Basal Bodies.  
In: Thomas Müller-Reichert, editor,  
Methods in Cell Biology (Volume 96).  
Academic Press, 2010, p. 117.  
ISBN: 978-0-12-381007-6  
© Copyright 2010, Elsevier Inc.  
Academic Press.

---

---

CHAPTER 6

Electron Tomography and  
Immuno-labeling of *Tetrahymena thermophila*  
Basal Bodies

**Thomas H. Giddings Jr., Janet B. Meehl, Chad G. Pearson,  
and Mark Winey**

Department of Molecular, Cellular and Developmental Biology, University of Colorado, Boulder,  
Colorado 80309

- 
- Abstract
- I. Introduction
  - II. Rationale
  - III. Methods
    - A. Asynchronous and Synchronous *Tetrahymena* Culture
    - B. High-pressure Freezing and Freeze-substitution of Cells
    - C. Chemical Fixation
    - D. Immuno-labeling Thin Sections
    - E. Electron Tomography
  - IV. Instrumentation and Materials
    - A. Culture and Synchronization Media
    - B. High-pressure Freezing and Freeze-Substitution
    - C. Immuno-labeling Thin Sections
    - D. Electron Tomography
  - V. Discussion
    - A. Synchronization of the Cell Cycle to Control Basal Body Duplication
    - B. Fixation
    - C. Electron Tomography
    - D. Concluding Remarks
- Acknowledgments
- References

---

---

---

**Abstract**

Basal bodies and centrioles are highly ordered, microtubule-based organelles involved in the organization of the mitotic spindle and the formation of cilia and flagella. The ciliate *Tetrahymena thermophila* has more than 700 basal bodies per cell, making it an excellent choice for the study of the structure, function, and assembly of basal bodies. Here, we describe methods for cryofixation of *Tetrahymena* by high-pressure freezing and freeze-substitution (HPF/FS) for the analysis of basal body structure with advanced electron microscopy techniques. Electron tomography of semi-thick HPF/FS sections was used to generate high-resolution three-dimensional images and models that reveal the intricate structure of basal bodies and associated structures. Immuno-labeling of thin sections from the same HPF/FS samples was used to localize proteins to specific domains within the basal body. To further optimize this model system, we used cell cycle synchronization to increase the abundance of assembling basal bodies. The *Tetrahymena* genome has been sequenced and techniques for genetic manipulations, such as construction of gene deletion strains, inducible expression and epitope tagging of proteins are now available. These advances have helped to make *Tetrahymena* a tractable experimental model system. Collectively, these methods facilitate studies of the mechanism of basal body assembly, the functions of basal body constituents and the cytological role of the basal body as a whole.

---

---

---

**I. Introduction**

Centrioles primarily serve two functions in cells. They comprise the core of centrosomes and mitotic spindle poles, and they act as basal bodies (BB) to template the formation of cilia. Regardless of their cytological role or cell type, the basic structure, consisting of a cylinder of microtubules arranged in 9-fold symmetry, is highly conserved (Beisson and Wright, 2003). A number of ciliated or flagellated cell types have been developed as model systems to investigate centriole and BB structure, function and mechanism of assembly (e.g. Marshall and Rosenbaum, 2000; O'Toole *et al.*, 2007; Pearson and Winey, 2009). In particular, *Tetrahymena thermophila* are single-cell, motile, ciliated protists containing approximately 750 basal bodies per cell. Here, we present methods to analyze the structure of assembling and mature *T. thermophila* BBs at high resolution and in three dimensions. These methods can be combined with molecular techniques to investigate the structure and function of components by gene disruption and localization of tagged proteins.

Approximately 600 basal bodies are aligned in rows in the cortical cytoplasm of *T. thermophila* to form the cilia responsible for motility (Fig. 1). About 150 more are tightly packed in the oral apparatus, a cavity involved in nutrient uptake. In *Tetrahymena* and other ciliates, cortical basal bodies anchor a complex network of cytoskeletal elements arrayed in a reiterated pattern. Each basal body nucleates the microtubules (MTs) of the ciliary axoneme and is associated with at least two other

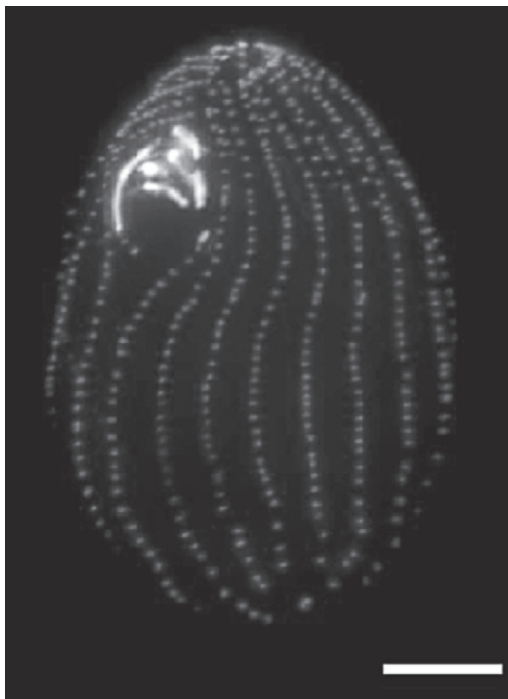


**Fig. 1** Immuno-fluorescence micrograph of a *Tetrahymena* cell labeled with an antibody to centrin, a pan specific marker for BBs (Stemm-Wolf *et al.*, 2005). Cortical rows of BBs run the length of the cell. The oral apparatus is located near the anterior of the cell (top). Scale bar = 10  $\mu$ m.

MT arrays, the transverse MTs and the post-ciliary MTs (Allen, 1969; Dippell, 1968; Iftode and Fleury-Aubusson, 2003). Mature *Tetrahymena* BBs are approximately 200 nm in diameter and 600 nm in length (Fig. 2). The proximal end is defined as the base, located in the cytoplasm facing the cell center, and the distal end is linked with the cilium (Allen, 1969). The wall of the basal body is comprised of nine MT triplets arranged in a cylinder (Fig. 3). Near the proximal end, the triplets are noticeably angled toward the center. The innermost MT is designated the “a” tubule, the middle MT as “b” and the outermost as the “c” tubule (Fig. 3B). The a and b MTs of the basal body triplets are continuous with the outer doublet MTs of the cilia. A cartwheel-shaped structure occupies the center of the BB cylinder at the proximal end (Fig. 2). A long filamentous structure, the kinetodesmal (KD) fiber, attaches laterally to the proximal end of the BB (Fig. 3). The formation of new basal bodies begins near the site of attachment of the KD fiber (Fig. 3). An electron dense core occupies the central BB lumen extending from the cartwheel to the transition zone (Fig. 2). Near the cell surface, the transition zone (TZ) marks the distal end of the BB (Fig. 2). The outermost MT of each BB triplet terminates at the TZ. Distal to the TZ is the

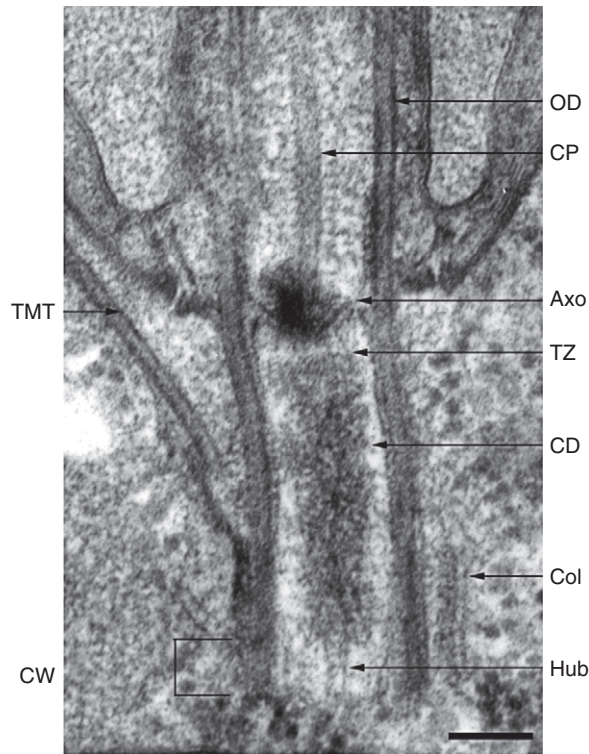


**Fig. 2** Electron micrograph of a longitudinal section through a cortical row BB and attached cilium from a HPF/FS-fixed *Tetrahymena* cell. The hub of the cartwheel (CW) is visible at the proximal end of the BB. The core density (CD) extends from the top of the CW nearly to the transition zone (TZ). On the distal surface of the TZ, an electron-dense area known as the axosome (Axo) anchors one of the central pair (CP) MTs of the cilium's axoneme. Outer doublet (OD) MTs of the axoneme are continuous with the triplet MTs that form the BB cylinder. Some of the structures associated with the proximal end of the BBs are visible in this image, including one of the transverse microtubules (TMT) and the collar (Col). The cell anterior is to the left in this view; HPF/FS thin section (Epon). Scale bar = 100 nm.

axoneme of the cilium. The central pair of MTs of the axoneme is anchored in an electron density known as the axosome on the distal side of the TZ.

In addition to making it possible to sample many BBs in a few micrographs, the large number of BBs and repetitive nature of the ciliary row organization make it feasible to find transient structures such as early stages of assembly. The position of new BBs relative to the mother BBs is predictable; they are always assembled on the anterior side at the proximal end. Synchronized cultures where most of the cells (> 95%) have a high frequency of assembling BBs enable straightforward identification of basal body assembly intermediates. The abundance of basal bodies in *Tetrahymena* makes this organism an excellent model system for ultrastructural analysis of basal body and cilia biogenesis. Often multiple BBs can be viewed in cross section at

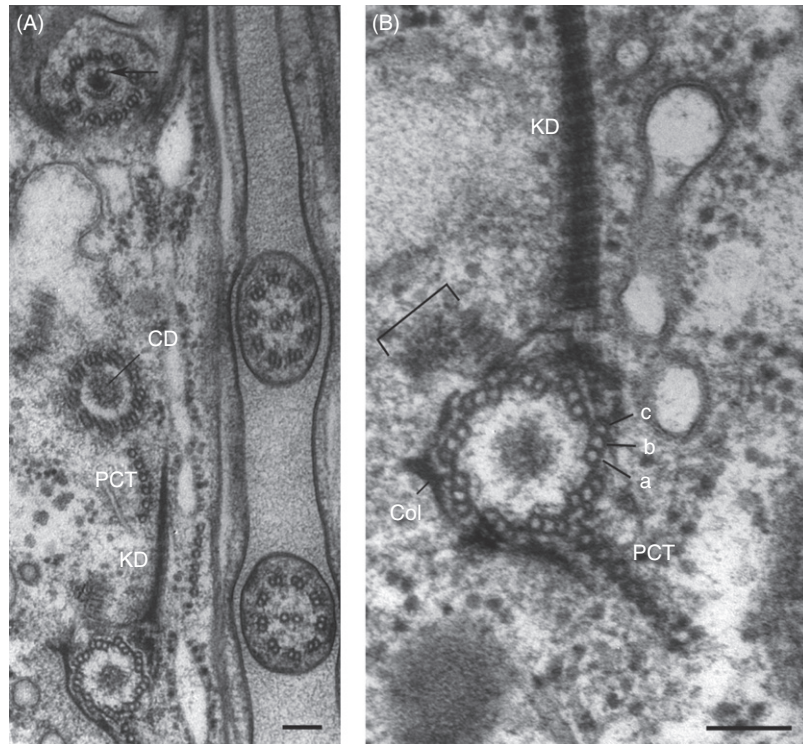


**Fig. 3** Cortical row BBs in cross section. (A) Three BBs in a cortical row (left side) and two cilia (right side) are seen in cross section. A band of post-ciliary MTs (PCT) lies adjacent to each BB along the side facing the posterior of the cell. The KD fiber (KD) attaches to the anterior-facing side of the BB at the proximal end. The core density (CD) is visible in the lower two BBs. Part of the axosome and a single central pair MT (arrow) is visible in the upper BB. (B) Higher magnification view of a BB in cross section showing a KD fiber, post-ciliary MTs, some of the collar (Col) and the site of nascent BB assembly (bracket). The a, b, and c MTs of one of the BB triplets are identified; HPF/FS thin sections (Epon). Scale bars = 100 nm.

sequential levels along the long axis of the basal body in a single micrograph (Fig. 4). A number of molecular techniques have been developed in recent years that allow the use of *Tetrahymena* as a versatile model system for experimental cell biology (reviewed by Turkewitz *et al.*, 2002). The complete *Tetrahymena* genome has been sequenced (Eisen *et al.*, 2006) and genetic tools have been developed to construct strains with epitope-tagged gene products, inducible gene expression, and gene deletions (Bruns and Cassidy-Hanley, 2000a,b; Frankel, 2000; Gaertig and Kapler, 2000; Hai *et al.*, 2000; Malone *et al.*, 2008; Pearson and Winey, 2009; Pearson *et al.*, 2009b; Stemm-Wolf *et al.*, 2005; Yu and Gorovsky, 2000). Kilburn *et al.* (2007) have characterized a *Tetrahymena* BB proteome. In addition to the genetic tools, basal body duplication can be temporarily suppressed by cell cycle arrest or synchronized basal body amplification can be induced to maximize the frequency of BB duplication



**Fig. 4** Thin section through an oral apparatus showing BBs cross sectioned at different levels along their long axis. The basal bodies toward the right side of the image were sectioned through the cartwheel structure located at the proximal end. HPF/FS. Scale bar = 100 nm.

at a known time point (Pearson *et al.*, 2009b). Experiments related to basal body assembly, maintenance and turnover are now possible (Pearson and Winey, 2009).

## II. Rationale

The need for precise 3-D EM imaging of BBs in *Tetrahymena* is derived from their intricate internal structure, their dynamic nature, and the complexity of the associated cytoskeletal elements. *Tetrahymena* provides an excellent model system in which these features can be studied in the cellular context of basal body assembly and the defects that arise when specific molecular components are depleted. Here, we describe modified techniques for high-pressure freezing (HPF)/freeze-substitution (FS), combined with either immuno-electron microscopy (IEM) or electron tomography (ET) to study mature and assembling BBs in *Tetrahymena* cells. This combination of methods was used effectively to resolve fine structural detail within basal bodies and associated

structures in *Chlamydomonas* (O'Toole *et al.*, 2003, 2007) and to obtain high-resolution 3D models of centrioles in mitotic spindles in *Caenorhabditis elegans* (Müller-Reichert *et al.*, 2007). Although 3D BB models have been generated from reconstructions of serial sections of *Tetrahymena* cells (Allen, 1969), we believe that the cryo-fixation and ET methods described here yield more precise models and convey a better understanding of the complex 3D structure of mature and assembling BBs. These techniques can also be used to assess the ultrastructural phenotype of mutant BBs at high resolution.

---

---

### III. Methods

#### A. Asynchronous and Synchronous *Tetrahymena* Culture

Quiescent (G1) *Tetrahymena* cells exhibit very low rates of BB duplication, whereas there is a rapid increase in the number of basal bodies beginning early in cell division (Frankel *et al.*, 1981; Kaczanowski, 1978; Nanney, 1975; Pearson *et al.*, 2009b). Starved cultures were used to obtain a population of cells in G1 with no new BB assembly. Virtually all of the BBs observed in cells fixed directly from depleted or minimal media can be assumed to be mature. Alternatively, synchronized cell growth and division was obtained by releasing starved cells back into the cell cycle by the addition of rich media (Pearson *et al.*, 2009b). Fixation when most cells were in mitosis yielded a population of *Tetrahymena* cells with maximal numbers of basal body assembly events per cell.

1. *Asynchronous Cultures*: *T. thermophila* strains were grown in super proteose peptone (SPP) media to mid-log phase, approximately  $2 \times 10^5$  cells/ml, in a 30°C incubator without shaking.
2. *Synchronization of cell growth*: To arrest cells in G1, log-phase growing cultures were washed into starvation media (10 mM Tris, pH 7.4) and incubated at 30°C 12–14 h. Cells were fixed directly from starvation media to visualize cells with mature BBs. To visualize cells in which there is significant amplification of basal body assembly, starved cells were washed and cultured in fresh SPP. Assembly of new basal bodies peaks about 2 h after release into the rich medium (Pearson *et al.*, 2009a). A similar increase in the number of assembling basal bodies can be achieved by growing cultures to confluency or stationary phase, followed by re-feeding with the addition of an equal volume of  $2 \times$  SPP.

#### B. High-pressure Freezing and Freeze-substitution of Cells

HPF and FS of *Tetrahymena* specimens resulted in good preservation of basal body ultrastructure (Figs. 2–5) as well as overall cell structure (Meehl *et al.*, 2009). Staining of the finest structures, such as the transition zone and cartwheel, is often lighter but

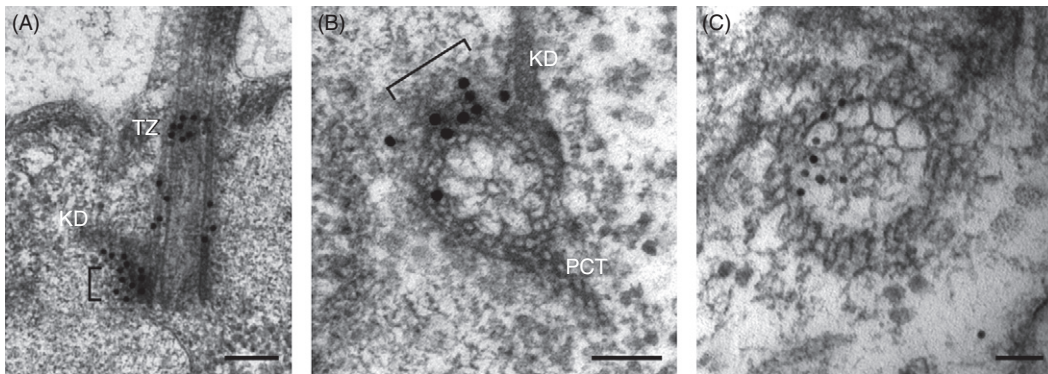


**Fig. 5** Immuno-electron microscopy using a polyclonal primary antibody specific to the basal body marker, Centrin (Cen1). Lowicryl HM20 sections prepared by HPF followed by FS in 0.25% glutaraldehyde and 0.1% UA in acetone were used. Cen1 localized primarily to the transition zone (TZ) and the site of nascent BB assembly (brackets) adjacent to the kinetodesmal fiber (KD). (A) Localization of Cen1 along the proximal–distal axis of a cortical basal body. Scale bar = 200 nm. (B) A cross section through the cartwheel at the proximal end of a cortical BB shows the radial distribution of Cen1. Post ciliary MTs (PCT). Scale bar = 100 nm. (C) High magnification view of the transition zone in cross section. Scale bar = 50 nm.

reveals more detail than in comparable views of chemically fixed cells. The difference is most apparent when thin tomographic sections are compared (Fig. 6).

1. *HPF*: 8–10 ml of log phase or synchronized *Tetrahymena* culture was centrifuged in a 15 ml conical centrifuge tube at  $500 \times g$  for 2 min. The supernatant was quickly removed from the pellets to prevent cells from swimming out of the pellet. The pellet was gently resuspended in 0.5 ml of a cryoprotectant solution consisting of SPP media supplemented with 15% dextran and 5% bovine serum albumin (BSA). After centrifugation at  $800\text{--}1000 \times g$  for 4 min, the supernatant was removed, leaving a minimal residue of cryoprotectant media with the pellet. This allows the cells to resuspend slightly, resulting in separation between cells. Cells that are loosely packed retain their normal shape, freeze better, and retain more of their cortical cilia. Two to three microliters of cells were loaded into the 100  $\mu\text{m}$  deep well (shallow side) of an aluminum Type B specimen carrier (Technotrade International) by pipette. After loading the cells under a dissecting microscope and confirming that the cells were still actively swimming, the sample was capped with a Type A specimen carrier. The flat side of the specimen carrier was coated with hexadecene (Sigma-Aldrich, St. Louis, MO, USA) for easier separation of the two pieces after HPF. We find it quicker and easier to have the Type B specimen carrier placed into the HPF's specimen holder before loading the cells. The holder's clamp is closed and tightened gently before inserting into the HPF. Working in an open tray of liquid nitrogen, HPF samples were transferred to cryovials containing 1 ml of FS medium. The samples lie on top of the frozen FS medium and sink down into it once the vial is warmed to initiate FS.

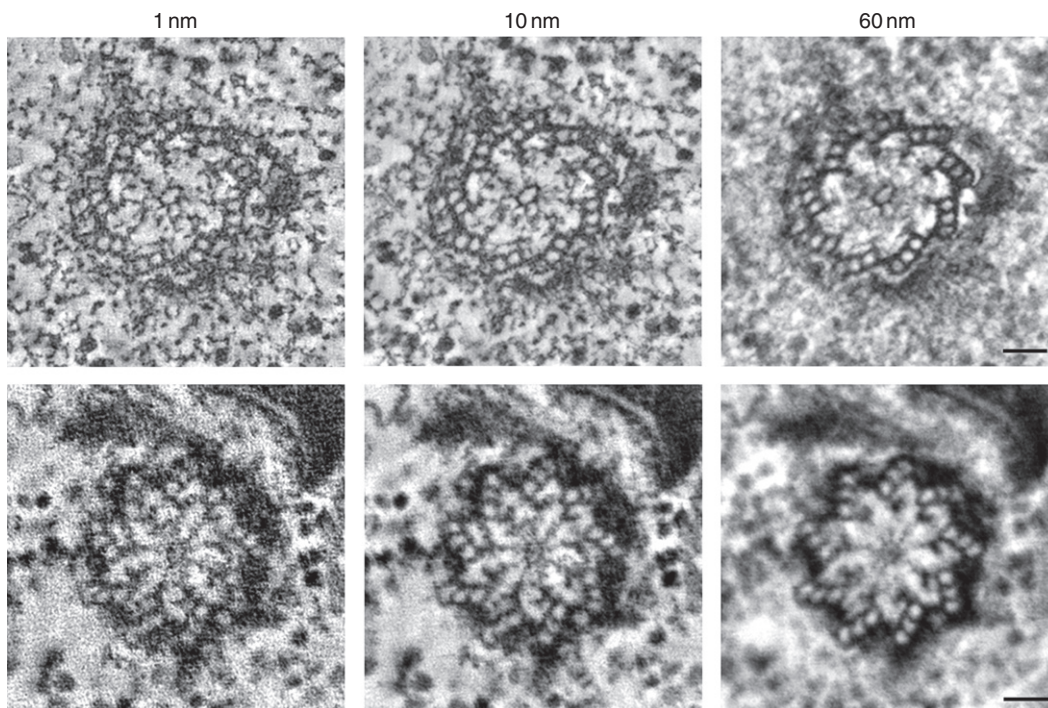


**Fig. 6** Comparison of high-pressure frozen cells and conventional chemically fixed cells by electron tomography. Using IMOD Slicer, the thickness, or Z-dimension, of the volume being viewed may be adjusted to simulate sections of variable thickness. Top row. HPF/FS cortical row basal body viewed in cross section at 1, 10, and 60 nm thicknesses. The finest details of the triplet MTs and cartwheel are best resolved in thinner tomographic slices. (HM20). Scale bar = 50 nm. Bottom row. A chemically fixed cortical row basal body in tomographic cross sections representing 1, 10, and 60 nm thick volumes. The fixation is good but fine details are more difficult to resolve due to the grainy or fuzzy appearance of BB structures; (chemical fixation, Epon). Scale bars = 50 nm.

2. *FS*: We currently employ two *FS* protocols for fixation and embedding of high-pressure frozen *Tetrahymena* cells (Meehl *et al.*, 2009). One uses *FS* in osmium tetroxide ( $\text{OsO}_4$ ) and uranyl acetate (UA) in acetone followed by embedding in Epon-Araldite to achieve a comprehensive, thorough fixation and stronger staining of both membranous and cytoskeletal organelles. The other is a milder fixation with glutaraldehyde and UA in acetone followed by embedding in Lowicryl HM20. The Lowicryl low-temperature embedding method was initially chosen to optimize the retention of antigenicity for immuno-labeling plastic-embedded sections but we have found that it also yields excellent preservation of cellular ultrastructure for high-resolution EM analysis including tomography. We generally freeze enough samples for both *FS* protocols.

1. Freeze-Substitution in 2% Osmium Tetroxide and 0.1% Uranyl Acetate in Acetone Followed by Embedding in Epon-Araldite Epoxy Resin

Cryovials containing the FS media and samples were placed in a metal block cooled to  $-80^{\circ}\text{C}$ . The block with samples was nestled in a chest of dry ice and placed in a standard  $-20^{\circ}\text{C}$  freezer for 3–4 days. Samples were warmed gradually to  $-20^{\circ}\text{C}$  overnight by removing the lid from the box, allowing a small amount of the dry ice to evaporate. The samples, still in the metal block, were moved to  $4^{\circ}\text{C}$  for 4–6 h and finally to room temperature for 1 h. Alternatively, automated FS devices or  $-80^{\circ}\text{C}$  freezers may be used to maintain the desired temperature throughout FS. The FS media was removed and the samples were rinsed  $2\times$  with acetone. The freeze-substituted cells and cryoprotectant solution typically form a cohesive disc that either falls off or can be removed gently from the specimen carriers by means of dissecting needles or other sharp tools. It may be necessary to work under a dissecting microscope to retrieve any small fragments. Samples were rinsed again in fresh acetone, then infiltrated with increasing concentrations of Epon-Araldite resin (without DMP30 accelerator) diluted in acetone: 25% Epon in acetone overnight; 50% Epon 8–10 h; 75% Epon overnight; and two changes of 100% Epon during the next day. The samples were left in Epon with accelerator overnight, transferred to BEEM capsules with fresh embedding resin the next day, and placed in a  $60^{\circ}\text{C}$  oven for polymerization for at least 48 h.

2. Freeze-Substitution in 0.25% Glutaraldehyde and 0.1% Uranyl Acetate in Acetone Followed by Embedding in Lowicryl HM20

As above, samples were freeze-substituted at  $-80^{\circ}\text{C}$  for 3–4 days followed by gradual warming to  $-20^{\circ}\text{C}$  overnight. Acetone rinses and infiltration with increasing concentrations of Lowicryl HM20 in acetone were all done at  $-20^{\circ}\text{C}$ . After rinsing with acetone chilled to  $-20^{\circ}\text{C}$ , the FS samples were separated from the specimen carriers. The procedure for separating the specimens from the specimen carriers is the same as above except that chilled acetone is used. It is best to work quickly to minimize sample warming that can lead to extraction and potential morphological changes. Samples were immediately rinsed in fresh  $-20^{\circ}\text{C}$  acetone as soon as they were returned to the cryovial and were infiltrated with increasing concentrations of Lowicryl HM20 diluted in acetone: 25% HM20 in acetone overnight; 50% HM20 for 6–8 h; and 75% HM20 overnight. Samples were finally incubated in 100% HM20 for about 1.5 days. During that time, four changes with fresh resin were made to ensure that any residual acetone was removed. Embedding capsules were half filled with fresh HM20 before transferring the samples, then filled to the top and capped. Polymerization under UV illumination was carried out at  $-45^{\circ}\text{C}$  in a homemade device (see Section IV.B.1).

We have recently freeze-substituted high-pressure frozen *Tetrahymena* cells using only 0.1% UA in acetone. The rest of the procedure was identical to the glutaraldehyde/UA FS and HM20-embedding protocol. The resulting preparations were nearly indistinguishable in morphology from those generated using the glutaraldehyde/UA FS

media. In other systems, this has allowed us to obtain significant labeling of aldehyde-sensitive antigens (Pearson *et al.*, 2009b) whereas little or no label was visible after using the glutaraldehyde/UA FS protocol.

### 3. Notes on Ultramicrotomy and Staining

Epon or Lowicryl HM20 plastic resin block faces were trimmed to short, wide trapezoids to optimize both the number of cells per section and the number of serial sections per grid. Cells can then be easily tracked from one section to the next. Thin sections (50–70 nm) were picked up on copper slot grids and stained in 2% UA in 70% methanol for 6 min; rinsed in the same solvent and dried; then stained in Reynolds lead citrate for 4 min and thoroughly rinsed with water. Aqueous 2% UA stain yields a less intense and less grainy staining, making it a better choice for thick sections destined for tomography. For IEM, staining times for both UA and lead can be reduced to better visualize colloidal gold particles over electron dense structures.

### C. Chemical Fixation

We have used aqueous chemical fixation for relatively quick preliminary assessments of new experimental samples. We modified the method of Orias *et al.* (1983) in which cells are fixed in a mixture of glutaraldehyde and OsO<sub>4</sub>. Cells were gently pelleted and resuspended in 0.5 ml glutaraldehyde fixative (2% glutaraldehyde, 1% sucrose in 5 mM NaPO<sub>4</sub> buffer at pH 7.0). After 1–2 min, an equal volume (0.5 ml) of 2% OsO<sub>4</sub> in 20 mM NaPO<sub>4</sub> buffer was added. Cells were fixed in the mixture of glutaraldehyde and osmium for 10 min. After gentle centrifugation, the blackened fixative solution was removed and the cells were resuspended in 1 ml of 2% OsO<sub>4</sub> in NaPO<sub>4</sub> buffer for 30 min. The fixed cells were washed twice with 20 mM NaPO<sub>4</sub> buffer, pH 7.0. Storing samples overnight at 4°C in the NaPO<sub>4</sub> buffer seemed to reduce the presence of small particulate precipitate (presumably a glutaraldehyde–osmium reaction product). The fixed cells were washed in 50% ethanol for about 2 min, *en bloc* stained in 1% UA/70% ethanol for 10 min, then further dehydrated in 95% ethanol for 5 min. Dehydration was completed with two 5 min washes in 100% ethanol and two rinses (2 and 5 min) in propylene oxide (PO). The cells were infiltrated for 1 h in a 1:1 mixture of Epon-Araldite (without accelerator) and PO, 1 h in 3:1 Epon-Araldite:PO, and 6 h in Epon-Araldite-containing accelerator. Cells were pipetted into BEEM capsules, allowed to settle, and the capsules were filled with resin. The samples were polymerized 60°C for 2 days.

### D. Immuno-labeling Thin Sections

For IEM, primary antibodies to selected native proteins or to fused tags such as green fluorescent protein (GFP) were used to label sections of *Tetrahymena* cells prepared by HPF/FS and embedded in Lowicryl HM20 as described above. Longitudinal and cross sections of BBs were used to determine the localization of proteins

along the proximal–distal axis and radially (Fig. 5). In Figure 5A and B for example, intense labeling of centrin at the site of future BB assembly can be distinguished from other positions around the proximal end of the BB. For less-abundant proteins, data from many median longitudinal sections and serial cross sections have been combined by placing a dot on a simple schematic map of a basal body for each secondary gold particle observed on a basal body in the TEM, making it possible to discern the localization pattern (Kilburn *et al.*, 2007; Pearson *et al.*, 2009b). Sections of lightly fixed cells embedded in LR White have also been used for immuno-localization studies in *Tetrahymena* (Ueno *et al.*, 2003).

We used established IEM methods for these studies of *Tetrahymena* BB proteins (Meehl *et al.*, 2009). Serial thin sections (50–70 nm) of Lowicryl-embedded cells on Formvar-coated nickel slot grids were placed, section side down, onto 15  $\mu$ l drops of blocking solution for 30 min, followed by 2 h on primary antibody diluted in blocking solution. Grids were rinsed with a steady stream of phosphate-buffered saline with Tween (PBST) for 20 s then labeled with an appropriate secondary antibody, generally 10 or 15 nm colloidal gold conjugated to goat-anti-rabbit or anti-mouse immunoglobulin for 1 h. Grids were rinsed first with PBST, then with distilled water, and finally carefully blotted and allowed to dry. To improve the visibility of colloidal gold secondary antibody on the basal bodies and associated structures, we use thinner sections and reduced staining times, usually less than 3 min with 2% aqueous UA, and 1 min with Reynolds' lead citrate.

Expression of GFP-fusion proteins is a versatile and valuable technique for the study of *Tetrahymena* BBs. We have used fluorescence microscopy of living *Tetrahymena* cells to identify new basal body components (Kilburn *et al.*, 2007), monitor changes in the number and distribution of BBs under various experimental conditions, and follow the incorporation and turnover of tagged BB components (Pearson *et al.*, 2009b). To date, we have used two GFP rabbit polyclonal antibodies (see Section IV.B.2), both of which give a strong signal with very low background following this IEM protocol.

A fundamentally different approach to mapping the distribution of proteins within BBs is *in situ* labeling of isolated pellicles, cell cortices that retain a high percentage of their BBs. Unfixed or very lightly fixed pellicles can be used, allowing the antibodies to recognize proteins in a near native state. Many more antigens are exposed to antibodies than with plastic-embedded sections. However, there is clearly a potential for loss of BB proteins under these conditions. For the *in situ* localization of BB proteins, pellicles were prepared as described in Kilburn *et al.* (2007), based on the methods of Nozawa and Thompson (1971). Cells were lysed in ice-cold buffer with a Dounce homogenizer and the cell lysate was fractionated on a sucrose step gradient. Alternatively, pellicles were prepared according to Coue *et al.* (1991). Pellicles were incubated in a range of dilutions of primary antibody in PBS, thoroughly rinsed in PBS, and incubated in 5 nm gold anti-rabbit immunoglobulin (or other appropriate secondary antibody). Use of a small size colloidal gold yields a stronger overall signal and may give a more accurate labeling pattern due to better penetration into and around basal bodies and easier removal of unbound secondary antibody. Following antibody

incubation, pellicles may be fixed with the same glutaraldehyde and osmium fixation used for whole cells, dehydrated in acetone, and embedded in Epon-Araldite resin (Suppl. Fig. A at <http://www.elsevierdirect.com/companions/9780123810076>).

### E. Electron Tomography

A 300 KV intermediate-voltage electron microscope (IVEM) was used to obtain a series of tilted views collected from semi-thick (200–300 nm) sections that are then compiled into high-resolution tomograms. Sections of 200–250 nm thickness are optimal because the ability of the IVEM to penetrate the sample and resolve detail in three dimensions is retained (Mastronarde, 1997), while the number of sections and corresponding tomograms to be combined is kept to a minimum. The best strategy is to use these thicker sections to reduce distortions and information loss within the reconstructed volume due to physical damage at each section interface. Since basal bodies almost always span more than one 250 nm section, dual axis tilt series were collected from each section in which a part of the basal body was present. Data sets can be collected from both longitudinal sections and cross sections of *Tetrahymena* basal bodies. The whole basal body can be captured in fewer sections in the longitudinal orientation than in cross section. However, the cross sections reveal more detail in the cartwheel structure as well as the transition zone (Figs. 7 and 8). Data from both orientations are useful for optimal visualization of basal body structure in the context of the cortical rows (Fig. 7).

Prior to undertaking ET of a new sample, we assessed the quality of fixation by conventional transmission electron microscopy (TEM) of thin sections. To prepare samples for tomography in the IVEM, serial semi-thick sections (200–250 nm) were cut and placed onto copper/rhodium slot grids (Electron Microscopy Sciences, Hatfield, PA, USA) coated with 0.7% Formvar. It is important to collect serial sections of consistent, known thickness to accurately calculate the sample volume in the final tomogram. The semi-thick sections require longer post-stain times than thin sections, 8 min in 2% aqueous UA and 5 min in Reynolds lead stain. Fifteen nanometer gold particles serve as fiducial markers for alignment of the tilt series images collected for tomography (O'Toole *et al.*, 2007). Droplets (5  $\mu$ l) of 15 nm colloidal gold (BBI, Intl., Cardiff, UK) were placed onto each side of the grid for 5 min. The droplets were gently wicked away with a Kimwipe and the grids were allowed to dry for 30 s. Excess salt was rinsed from the grids by applying 5  $\mu$ l of water to each side of the grid and the droplet was wicked away immediately using a Kimwipe. If there is a hole in the Formvar, droplets will not remain confined to one side of the grid and the sample as a whole will be very unstable under the electron beam. Damaged grids were “repaired” by floating a new Formvar film on water and placing the grids section side down, onto the film. Grids were then retrieved and freed from the surrounding Formvar film.

The plane of section through a basal body has a significant impact on the resolution of fine structural detail within or around the basal body, making it desirable to

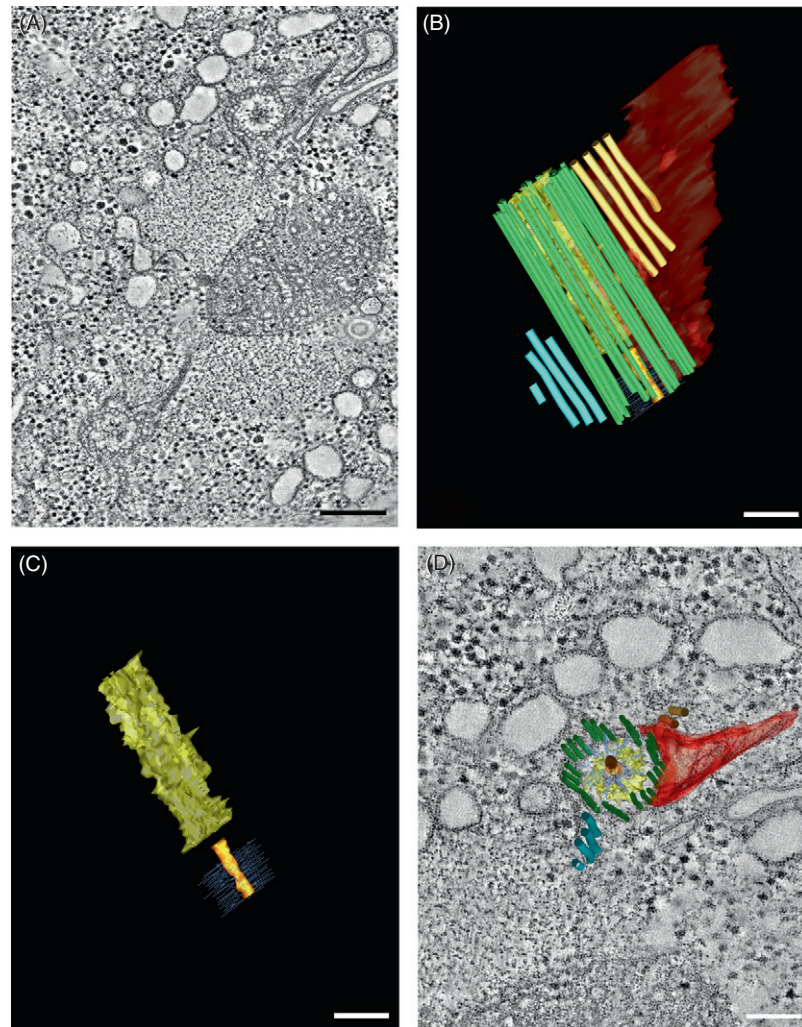


**Fig. 7** A tomogram and 3D projections of modeled cortical row basal bodies. The basal body itself is composed of many structures. The cylinder walls are constructed of nine sets of triplet microtubules (green), a hub (orange) and spokes (periwinkle) radiating from the hub form the cartwheel located at the proximal end of the basal body. Distal to the cartwheel is the core density (yellow). Other cytoskeletal structures are associated with the BBs in the cortical rows. The kinetodesmal fiber (red) attaches to the proximal end of the BB. The post-ciliary MTs (blue) and the transverse MTs (tan) are located on opposite sides of the BB. The spatial relationships among these structures are more easily visualized by rotating the models (supplemental movie—[Fig. 7 model.mov](http://www.elsevierdirect.com/companions/9780123810076) at <http://www.elsevierdirect.com/companions/9780123810076>, scale bar = 100 nm). (A) Tomographic slice displaying two BBs in a cortical row; HPF/FS (Os, Epon) tomogram. Scale bar = 200 nm. (B) A 3D projection of modeled features of one of the cortical row BBs. Scale bar = 100 nm. (C) Certain contours may be removed to reveal internal structures of the BB such as the core density and cartwheel. Scale bar = 100 nm. (D) The 3D projection model superimposed on the tomographic slice ties together the modeled structures with the actual structures. Scale bar = 100 nm. (See Plate no. 7 in the Color Plate Section.)

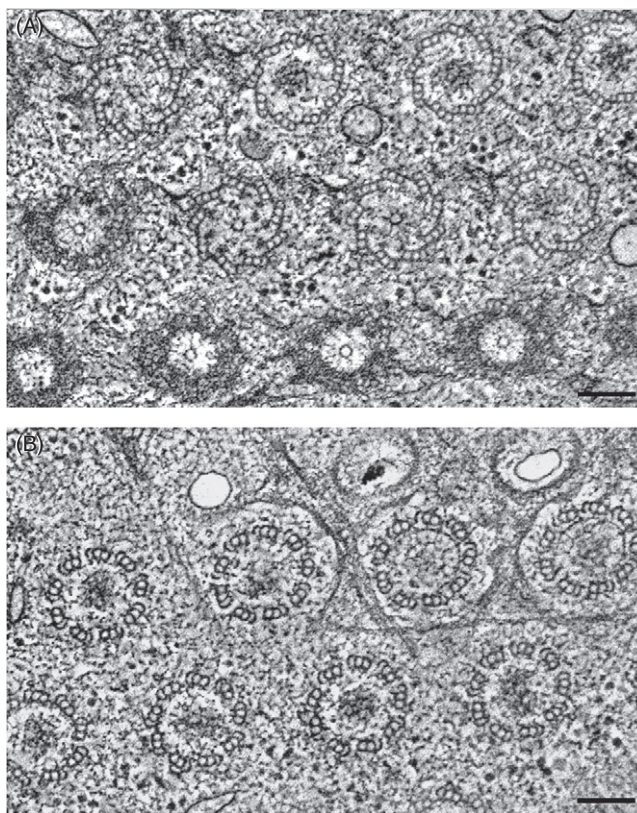


**Fig. 8** Computed image slices from a WT *Tetrahymena* oral apparatus tomogram. Within one tomographic slice, many cross-sectional views of the BB are represented. (A) The hub and spokes of the cartwheel are visible in the BBs of the bottom row. The triplet microtubules and the cartwheel are well defined in the middle row and the BBs in the top row are transected through the mid-region where the core density resides. (B) In a more distal tomographic slice of the same oral apparatus, the fine lacy structure of the transition zone (TZ) is visible in the center of the two BBs on the right side of the top row; HPF/FS (HM20) tomogram. Scale bars = 100 nm. A movie of the whole tomogram is available for viewing (supplemental movie—Fig.8 tomo.mov at <http://www.elsevierdirect.com/companions/9780123810076>, scale bar = 200 nm).

first search for basal bodies of interest that happen to be favorably oriented within the section. This can be achieved by previewing the semi-thick sections in a standard TEM at 100 KV. Low magnification images are used to map the chosen basal bodies of specific cells. Errors in tracking a selected basal body from section to section can easily occur due to the reiterated nature of the basal bodies and associated cytoskeletal elements. Non-cytoskeletal features of the cortical cytoplasm, such as mitochondria and vacuoles can be used as large-scale fiducial landmarks. Time spent previewing a given grid on a 100 KV TEM can save a significant amount of time on the IVEM.

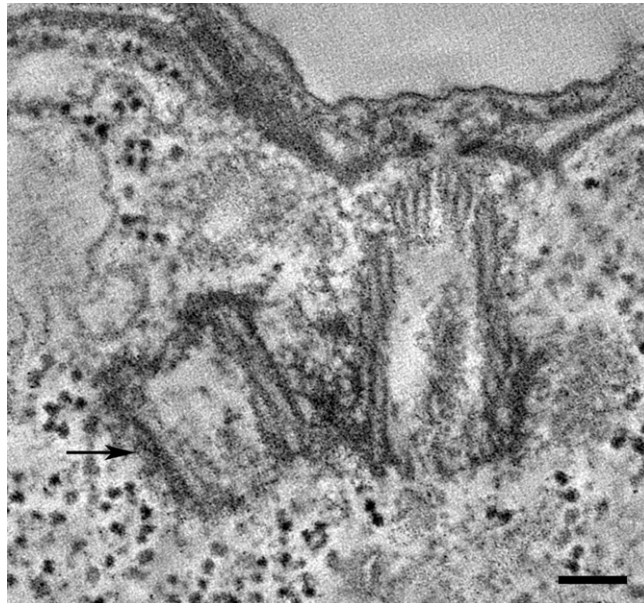


**Fig. 9** Longitudinal view of new basal body assembly. The cells were starved and released and then chemically fixed at selected time points to generate samples enriched for stages of new basal body assembly. The new basal body (arrow) arises on the anterior side of the mature basal body; Chemical fixation, tomographic slice. Scale bar = 100 nm.

The methods of image acquisition and tomogram generation are described in O'Toole *et al.* (2007) and Chapter 4 by O'Toole (this volume). Images were collected at  $1^\circ$  increments from  $+60^\circ$  to  $-60^\circ$  using a Technai F30 IVEM equipped with a eucentric stage, SerialEM software (available from the Boulder 3D EM Lab website: <http://bio3d.colorado.edu>) and Digital Micrograph software (Gatan, Inc., Pleasanton, CA). SerialEM automates the stage tilt, sample tracking, and sample autofocus (Mastronarde, 2005). After collection of the first tilt series around one axis, referred to as the "A stack," the grid is rotated  $90^\circ$  and images of the same area are collected for the second tilt series around the orthogonal axis, called the "B stack." Since the grid cannot be rotated through  $\pm 90^\circ$  range, dual axis data sets are collected to minimize the effect of the "missing wedge" of information when the images are processed to generate tomograms (Mastronarde, 1997).

A set of programs collectively known as the IMOD software package (Kremer *et al.*, 1996; Mastronarde, 1997) is used to generate a tomogram from the dual axis tilt series data. A graphical user interface, eTomo, manages the set of IMOD programs used to align the tilt series data and generate the tomograms. First, a pre-processing step

eliminates pixels of extreme intensity caused by X-rays. Next, the images in the data set are coarsely aligned based on X and Y translational cross correlation and a temporary coarsely aligned stack is generated. Following the coarse alignment of the stack, a seed model is generated using the image display and modeling program, 3dmod. Fiducial markers are chosen by adding contours over 20–40 gold particles at the 0° tilt view. These fiducial markers should be distributed equally over the viewing area as well as on both sides of the section. The gold particles are then automatically tracked through the entire stack and their model positions are used for the fine alignment. The user corrects fiducial model points that need adjustment to improve the alignment. Other factors such as magnification changes, tilt axis rotation, translation shifts, and distortion are corrected when this program is executed. A fully aligned stack is generated and a tomogram is produced. The same process is repeated to generate a tomogram from the B stack data. Tomograms from both axes are then aligned and combined to generate a final, dual-axis tomogram (Figs. 6–9 and supplemental movies).

Tomograms were generated for each section and then combined using the Join interface in eTomo. Details of this procedure can be found in Höög and Antony (2007). To begin, the tomograms were manually aligned with each other by aligning sample slices from the top of one tomogram with the bottom of the adjacent tomogram. A model was then generated to refine the alignment of the serial tomograms. For example, a microtubule may continue from one section into the next. A contour is traced along the length of the microtubule contained in each section. MTs are more easily visualized by using a tool called Slicer, in which a 3D volume is extracted from the tomogram and rotated in X, Y, or Z to best visualize the MT along its length. Model points are placed along the microtubule fragments from adjacent sections and these contours are joined together; the more contours that are joined across a boundary, the better the alignment. The aligned tomograms were then rejoined into a combined volume and the model was transformed to fit the new tomogram. The 3dmod program was used to model features of interest in the joined tomogram (Fig. 7B). Fine substructures within the BB were modeled (Fig. 7C and supplemental movie Fig. 7 model.mov at <http://www.elsevierdirect.com/companions/9780123810076>) along with the BB triplet MTs (green), post-ciliary MTs (blue) and transverse MTs (tan), and the KD fiber (red). Overlaying the model on the tomogram is a useful tool to correlate the model with the actual biological sample (Fig. 7D).

---

---

---

## IV. Instrumentation and Materials

### A. Culture and Synchronization Media

*Materials:* *T. thermophila* strain B2086 and CU428 (for construction of knockout strains), Tetrahymena Stock Center, Cornell University.

*Media:* SPP media [2% proteose peptone, 0.1% yeast extract, 0.2% glucose, 0.003% Ferric EDTA supplemented with antibiotic/antimycotic mix (100 units/ml penicillin,

100 µg/ml streptomycin, 0.25 µg/ml amphotericin B (fungizone)]; Starvation media [10 mM Tris, pH 7.4]; 2× SPP was prepared for adding to cultures of starved cells. The final medium for re-feeding was 1× SPP.

## B. High-pressure Freezing and Freeze-Substitution

### 1. Instrumentation

High-pressure freezers: General techniques for HPF have been described (e.g., Dahl and Staehelin, 1989; Gilkey and Staehelin, 1986; McDonald, 1999, 2007; Moor, 1987). We use a Bal-Tec HPM 010 (currently available from RMC, Tucson, AZ). Other available models include the Wohlwend HPM 01 (available in the USA through Technotrade International, Manchester, NH) and two models from Leica, the Leica EM PACT2 (McDonald *et al.*, 2007) and the Leica EM HPM100.

FS system: A Styrofoam box filled with dry ice was used to maintain the samples at −80°C for initial FS and was placed in a standard refrigerator-freezer unit for intermediate temperatures and low-temperature embedding. We used a metal block with holes drilled in it to hold the cryovials of FS media upright and to provide a slower rate of temperature change during warming from −80 to −20°C.

Our UV polymerization chamber is a homemade insulated box with two 7-watt UV lights mounted into the lid. BEEM capsules with samples in liquid resin are held in a wire rack immersed in a temperature-controlled bowl of isopropyl or methyl alcohol. Dry ice is placed in the bottom of the box and the temperature is maintained at −45°C by means of a thermocouple-based controller and a heating element wrapped around the bowl. Commercially available alternatives include automated freeze substitution devices such as the Leica EM AFS (Leica Microsystems, Vienna, Austria). These are versatile and convenient means of achieving controlled, reproducible FS and UV polymerization of low-temperature embedding resins. These units have the advantage of offering a wide range of temperatures for initial FS, low-temperature fixation, resin infiltration and polymerization, and controlled rates of temperature change throughout the protocol.

### 2. Materials

Cryoprotectant solutions for HPF: 15% dextran (Avg. MW 9.5 KD, Sigma), 5% BSA in SPP was used. We have evaluated the quality of freezing of *Tetrahymena* cells achieved by using a variety of cryoprotectants. Lower MW dextran (9.5–11 KD) is less viscous at the same concentration than the more typically used 40 KD dextran, permitting easier handling of the *Tetrahymena* cells. The most consistent results were obtained with a mixture of 15% dextran (Avg. MW 9.5 KD; Sigma) and 5% BSA in culture media; 18% dextran in SPP also produced samples free of detectable ice crystal damage in freeze-substituted samples. Factors considered in choosing the cryoprotectant included not only quality of freezing but also ease of embedding, sectioning, and staining; 20% dextran, for

example, typically yields very good freezing but apparently surrounds the cells in a hydrophilic shell that retards penetration of fixatives and embedding resin. The results of poor embedding include a block face that attracts water during sectioning and sections that expand or disintegrate on the boat of the microtome knife.

Specimen carriers: Type A and Type B aluminum specimen carriers were purchased from Technotrade International and are available from several sources. These and many other styles of specimen carriers have been reviewed (McDonald *et al.*, 2007). Use of the 100  $\mu\text{m}$  deep well gave consistently better freezing than deeper wells. In addition, the discs of sample exhibited a more uniform and clear color after FS presumably indicating thorough FS and penetration of the fixatives.

FS media for Epon embedding: 2%  $\text{OsO}_4$  and 0.1% UA in acetone was prepared by placing 12.25 ml of anhydrous acetone in a vial and using 1 ml of the acetone to dissolve the 0.25 g  $\text{OsO}_4$  in a glass ampoule (EMS: Electron Microscopy Sciences, Hatfield, PA). The dissolved osmium was returned to the vial and placed on dry ice. Repeating the process quickly dissolved all of the  $\text{OsO}_4$ ; 0.25 ml of 5% UA (EMS) in methanol (stored at  $-20^\circ\text{C}$ ) was added to the solution. The FS mixture was kept on dry ice until it was aliquoted (1 ml/vial) to 1.8 ml cryovials (Nalge Nunc International, Rochester, NY, USA), which were then stored under liquid nitrogen until needed.

FS media for Lowicryl HM20 embedding: 0.25% glutaraldehyde and 0.1% UA in acetone was prepared by adding 0.25 ml 10% glutaraldehyde in acetone (EMS) and 0.2 ml of a 5% UA/methanol stock solution to 9.55 ml acetone. The FS media was then aliquoted to cryovials as described above.

### C. Immuno-labeling Thin Sections

#### 1. Equipment

Immuno-labeling was done in a covered glass Petri dish lined with moist filter paper and Parafilm. The droplets of blocking solution and antibodies were placed on the Parafilm and the dish was set on a magnetic stir plate. The speed of the stirrer is adjusted to provide very slow rotation of the nickel grids. Non-magnetic-self-closing tweezers are useful for handling nickel grids.

#### 2. Reagents

1. PBST: 10 mM sodium phosphate, 150 mM sodium chloride, and 0.1% Tween 20.
2. Blocking solution: 1% nonfat dry milk powder was dissolved in PBST, vortexed, and allowed to stand for 5 min, then centrifuged at  $1500 \times g$  to remove undissolved solids.
3. Primary polyclonal antibodies to GFP were generous gifts from M. Rout (Rockefeller University, New York, NY) or P. Silver (Dana Farber Cancer Institute, Boston, MA). Goat-anti-rabbit-15 nm gold or 10 nm gold (Ted Pella, Redding, CA) secondary antibodies were diluted 1:20 in blocking solution.

#### D. Electron Tomography

IVEM: Semi-thick (200–300 nm) sections were imaged in an IVEM equipped with an automated serial tilt goniometer and a rotating specimen holder. We use a TECNAI F30 FEG at the Boulder Laboratory for 3D Electron Microscopy of Cells (website: <http://bio3d.colorado.edu>). Tilt series were captured using Serial EM software. 3D reconstruction and modeling were accomplished with the aid of IMOD. These programs were developed by, and may be obtained from, the Boulder 3D EM Lab (website: <http://bio3d.colorado.edu>).

100 KV TEMs: FEI-Philips CM10 or CM100 operated at 80 KV for thin sections (50–100 nm) or 100 KV for previewing semi-thick sections for ET. These and most other research-grade TEMs are equipped with  $\pm 60^\circ$  goniometers for tilting specimens. A specimen holder capable of rotating grids can be used to align BBs or other structures on a desired tilt axis, such as for viewing the triplet MTs of the BB in perfect cross section. With the abundance of BBs in *Tetrahymena* cells, we often found it to be more efficient to simply search around for optimal views.

---

---

---

#### V. Discussion

High-resolution, 3D electron microscopy is needed to generate accurate depictions of the intricate structure of BBs. This serves as the basis for the precise mapping of constituent proteins, the models of assembly, and the elucidation of the functions of those molecules and of the BB as a whole. The application of methods for manipulating *Tetrahymena* cultures to produce cells in predictable stages of the basal body cycle, using HPF/FS methods of specimen preparation to faithfully preserve the structures, and the use of 3D imaging techniques are discussed below. We have employed these methods to study the assembly of new BBs in *Tetrahymena*. This allows for analysis of the phenotypes resulting from mutations in basal body constituent proteins and the localization of those proteins.

##### A. Synchronization of the Cell Cycle to Control Basal Body Duplication

Basal bodies are dynamic structures. In addition to initial assembly and subsequent maturation, basal body proteins continuously turn over at their binding sites (Pearson *et al.*, 2009a). The simple method of nutrient removal described here was used to ensure that all of the basal bodies being monitored for protein turnover were not newly assembled during the experiment. Conversely, synchronization by starvation followed by re-feeding enabled us to find cells with a high frequency of assembling basal bodies. From fluorescence images and stained cells, it is known that the highest frequency of duplication occurs in the midzone of *Tetrahymena* cells during the early stages of cell division (Frankel *et al.*, 1981; Kaczanowski, 1978; Nanney, 1975). Preparations from starved and released cultures allow visualization of BBs at a range of stages of assembly

in both wild-type (Fig. 9) and mutants. In addition, this enables the determination of the timing of incorporation of selected proteins.

## B. Fixation

Traditional chemical fixation of *Tetrahymena* and *Paramecium* cells with aqueous glutaraldehyde and OsO<sub>4</sub> generated a wealth of structural information about basal bodies, their duplication, and the associated cortical cytoplasm (Allen, 1969; Dippell, 1968; Iftode and Fleury-Aubusson, 2003; Iftode *et al.*, 1989, 1996; Jerka-Dziasosz *et al.*, 2001; Orias *et al.*, 1983; Sharma *et al.*, 2007). Following the successful application of HPF, FS, and tomography to the study of basal bodies and overall cytology in *Chlamydomonas* (O'Toole *et al.*, 2007; Chapter 4 by O'Toole, this volume), we sought to develop effective HPF/FS methods for *Tetrahymena* to generate similarly well fixed and stained cells for ET. We used chemical fixation in parallel with HPF/FS to monitor potential HPF artifacts and to determine whether any structural element was inadequately preserved or stained. Those results were used to modify cell harvesting and cryoprotectant composition for HPF (Meehl *et al.*, 2009). Mannitol, a monomeric sugar-alcohol used as a penetrating cryoprotectant in HPF protocols for *Chlamydomonas* (O'Toole *et al.*, 2007), caused plasmolysis and disruption of cellular organization in *Tetrahymena*. We replaced it with dextran, a high-MW glucose polymer. A mixture of 15% (w/v) dextran and 5% BSA dissolved in growth medium (SPP) yielded cryofixation that was free of detectable ice crystal damage and served as a stable but permeable encasement around the cells through FS and embedding.

Together with careful handling (minimal centrifugation for harvesting and gentle resuspension), use of this cryoprotectant medium resulted in reduced disruption of the cytoplasm and improved retention of cilia.

FS in the presence of OsO<sub>4</sub> in the FS media followed by embedding in Epon Araldite resulted in fixation that more closely resembles traditional room temperature, aqueous chemical fixation. Staining of both cytoskeletal elements and membranes was strong but frequently grainy, a significant problem when the samples were imaged by tomography. FS with low concentrations of glutaraldehyde and UA yielded high-quality ultrastructure with the added benefit of good preservation of antigenicity for IEM. We believe that the light staining of fine structure is less likely to mask fine detail and permits a higher resolution rendition of the structure.

## C. Electron Tomography

The complex cortical cytoskeleton of *Tetrahymena* makes it a desirable candidate for the use of 3D imaging techniques to understand the interrelationships of the various elements as well as the detailed structure of the basal bodies themselves. We know from immunofluorescence observations that mutants in basal body components display disrupted cortical row organization, underscoring the importance of 3D ultrastructural analysis of this system (Culver *et al.*, 2009; Pearson *et al.*, 2009b; Stemm-Wolf *et al.*,

2005). Although imaging serial thin sections plays an important role in viewing and analyzing this system, we found that ET provides superior detail and conveys 3D structure much more efficiently.

Tomographic slices and model projections derived from some of our tomograms are shown in Figs. 7 and 8. The tomograms and associated models are also presented as Quick Time movies (Supplemental Materials). The kinetodesmal fiber, transverse microtubules, and post-ciliary microtubules can be traced and modeled along with the basal body (Fig. 7). Projections of the model can be rotated in three dimensions to get a better idea of the spatial relationship of all the structures (supplemental movie—Fig. 7 model.mov at <http://www.elsevierdirect.com/companions/9780123810076>). Several components of the basal body itself are incorporated into the model, including the triplet MTs, the hub and spokes of the cartwheel at the proximal end of the basal body, and the core density (Fig. 7D).

Favorable cross sections through the BB-rich oral apparatus contain a wealth of information in a single tomogram. One tomogram can incorporate every cross-sectional view through a basal body. In Fig. 8A, the proximal end of the basal body is identified by the characteristic spoke and hub components of the cartwheel. The core density is clearly visible in several basal bodies, and distal to the core density, the lacey layers of the transition zone can be seen (Fig. 8B).

We believe that the ET methods described here permit the visualization, modeling, and understanding of *Tetrahymena* basal body and cytoskeleton organization in three dimensions at higher resolution and more effectively than traditional serial sectioning approaches. Chemical fixation was occasionally used to generate samples for ET and yielded some useful data. However, the cell ultrastructure had a grainy, fuzzy appearance. When compared to a HPF/FS sample (Fig. 6), the chemically fixed sample cannot be resolved to the same degree as the HPF sample. In addition to revealing the structure of mature, wild-type BBs at improved resolution, ET of HPF/FS *Tetrahymena* cells can now be used to describe the process of basal body assembly, examine basal body mutants, and detect abnormalities in the basal body accessory structure organization.

#### D. Concluding Remarks

Excellent 3D descriptions and models of mature and developing basal bodies in *Tetrahymena* (Allen, 1969) and *Paramecium* (Dippell, 1968; Ifode and Fleury-Aubusson, 2003; Ifode *et al.*, 1989, 1996) were generated 40 years ago from TEM of serial thin sections of chemically fixed cells. The goal of the cryofixation and ET methods described here is to push the preservation and resolution of *Tetrahymena* basal body structure to the molecular level. Following HPF/FS/ET, it is possible to more precisely visualize detail in many BB substructures such as the cartwheel, transition zone, site of duplication, and peripheral densities. Selected gene products can be localized to specific sub-domains within, or associated with basal bodies. A combination of immuno-localization and the comparison of deletion mutants to wild-type structures can now be used to identify the function of individual gene products and visualize the structures that they form at the molecular level. Following

experimental manipulation of the strains and cell culture conditions, the same methods can be used to visualize the assembly process, identify the order of assembly of the various basal body components, and reveal the mechanisms for the maintenance and modification of basal bodies.

## Acknowledgments

We thank Eileen O'Toole (Boulder Laboratory for 3D EM of Cells) for helpful advice and assistance with ET. Christina Clarissa provided excellent technical assistance and contributed some of the thin section images. Alex Stemm-Wolf provided the Cen1 antibody and immuno-fluorescence images and initiated many of the experiments. *Tetrahymena* work in the Winey lab is supported by NIH (RO1 GM74746) and by the March of Dimes Birth Defects Foundation (#1-FY07-422).

## References

- Allen, R. D. (1969). The morphogenesis of basal bodies and accessory structures of the cortex of the ciliated protozoan *Tetrahymena pyriformis*. *J. Cell Biol.* **40**, 716–733.
- Beisson, J. and Wright, M. (2003). Basal body/centriole assembly and continuity. *Curr. Opin. Cell Biol.* **15**, 96–104.
- Bruns, P. J. and Cassidy-Hanley, D. (2000a). Methods for genetic analysis. *Meth. Cell Biol.* **62**, 229–240.
- Bruns, P. J. and Cassidy-Hanley, D. (2000b). Biolistic transformation of macro- and micronuclei. *Meth. Cell Biol.* **62**, 501–512.
- Coue, M., Lombillo, V. A., and McIntosh, J. R. (1991). Microtubule depolymerization promotes particle and chromosome movement *in vitro*. *J. Cell Biol.* **112**, 1165–1175.
- Culver, B. P., Meehl, J. B., Giddings, T. H.Jr., and Winey, M. (2009). The two SAS-6 homologs in *Tetrahymena thermophila* have distinct functions in basal body assembly. *Mol. Biol. Cell* **20**, 1865–1877.
- Dahl, R. and Staehelin, L. A. (1989). High pressure freezing for the preservation of biological structure: Theory and practice. *J. Electron Microsc.* **13**, 165–174.
- Dippell, R. V. (1968). The development of basal bodies in paramecium. *Proc. Natl. Acad. Sci. USA* **61**, 461–468.
- Eisen, J. A., Coyne, R. S., Wu, M., Wu, D., Thiagarajan, M., Wortman, J. R., Badger, J. H., Ren, Q., Amedeo, P., Jones, K. M., et al., (2006). Macronuclear genome sequence of the ciliate *Tetrahymena thermophila*, a model eukaryote. *PLoS Biol.* **4**, e286.
- Frankel, J. (2000). Cell biology of *Tetrahymena thermophila*. *Meth. Cell Biol.* **62**, 27–125.
- Frankel, J., Nelsen, E. M., and Martel, E. (1981). Development of the ciliature of *Tetrahymena thermophila* II. Spatial subdivision Prior To cytokinesis. *Dev. Biol.* **88**, 39–54.
- Gaertig, J. and Kapler, G. (2000). Transient and stable DNA transformation of *Tetrahymena thermophila* by electroporation. *Meth. Cell Biol.* **62**, 485–500.
- Gilkey, J. C. and Staehelin, L. A. (1986). Advances in ultrarapid freezing for the preservation of cellular ultrastructure. *J. Electron Microsc. Tech.* **3**, 177–210.
- Hai, B., Gaertig, J., and Gorovsky, M. A. (2000). Knockout heterokaryons enable facile mutagenic analysis of essential genes in *tetrahymena*. *Methods Cell Biol.* **62**, 513–531.
- Höög, J. L. and Antony, C. (2007). Whole-cell investigation of microtubule cytoskeleton architecture by electron microscopy. *Meth. Cell Biol.* **79**, 145–167.
- Ifode, F., Adoutte, A., and Fleury, A. (1996). The surface pattern of *Paramecium tetraurelia* in interphase: An electron microscopic study of basal body variability, connections with associated ribbons and their epiplasmic environment. *Eur. J. Protistol.* **32**, 46–57.
- Ifode, F., Cohen, J., Ruiz, F., Torres-Rueda, A., Chen-Sban, L., Adoutte, A., and Beisson, J. (1989). Development of surface pattern during division in *paramecium*. I. Mapping of duplication and reorganization of cortical cytoskeletal structures in the wild type. *Development* **105**, 191–211.

- Iftode, F. and Fleury-Aubusson, A. (2003). Structural inheritance in *paramecium*: Ultrastructural evidence for basal body and associated rootlets polarity transmission through binary fission. *Biol. Cell* **95**, 39–51.
- Jerka-Dziadosz, M., Strzyzewska-Jowko, I., Wojsa-Lugowska, U., Krawczynska, W., and Krzywicka, A. (2001). The dynamics of filamentous structures in the apical band, oral crescent, fission line and the postoral meridional filament in *Tetrahymena thermophila* revealed by the monoclonal antibody 12G9. *Protist* **152**, 53–67.
- Kaczanowski, A. (1978). Gradients of proliferation of ciliary basal bodies and the determination of the position of the oral primordium in tetrahymena. *J. Exp. Zool.* **204**, 417–430.
- Kilburn, C. L., Pearson, C. G., Romijn, E. P., Meehl, J. B., Giddings, T. H., Jr., Culver, B. P., Yates, J. R.3rd, and Winey, M. (2007). New *tetrahymena* basal body protein components identify basal body domain structure. *J. Cell Biol.* **178**, 905–912.
- Kremer, J. R., Mastronarde, D. N., and McIntosh, J. R. (1996). Computer visualization of three-dimensional image data using IMOD. *J. Struct. Biol.* **116**, 71–76.
- Malone, C. D., Falkowska, K. A., Li, A. Y., Galanti, S. E., Kanuru, R. C., LaMont, E. G., Mazzarella, K. C., Micev, A. J., Osman, M. M., Piotrowski, N. K., Suszko, J. W., Timm, A. C., et al., (2008). Nucleus-specific importin alpha proteins and nucleoporins regulate protein import and nuclear division in the binucleate *Tetrahymena thermophila*. *Eukaryot. Cell* **7**, 1487–1499.
- Marshall, W. F. and Rosenbaum, J. L. (2000). How centrioles work: Lessons from green yeast. *Curr. Opin. Cell Biol.* **12**, 119–125.
- Mastronarde, D. N. (1997). Dual-axis tomography: An approach with alignment methods that preserve resolution. *J. Struct. Biol.* **120**, 343–352.
- Mastronarde, D. N. (2005). Automated electron microscope tomography using robust prediction of specimen movements. *J. Struct. Biol.* **152**, 36–51.
- McDonald, K. L. (1999). High-pressure freezing for preservation of high resolution fine structure and antigenicity for immunolabeling. *Methods Mol. Biol.* **117**, 77–97.
- McDonald, K. L. (2007). Cryopreparation methods for electron microscopy of selected model systems. *Meth. Cell Biol.* **79**, 24–52.
- McDonald, K. L., Morphew, M., Verkade, P., and Mueller-Reichert, T. (2007). Recent advances in high-pressure freezing: Equipment and specimen loading methods. *Methods Mol. Biol.* **369**, 143–173.
- Meehl, J. B., Giddings, T. H., and Winey, M. (2009). High pressure freezing, electron microscopy, and immuno-electron microscopy of *Tetrahymena thermophila* basal bodies. *Methods Mol. Biol.* **586**, 227–241.
- Moor, H. (1987). Theory and practice of high pressure freezing. In “Cryotechniques in Biological Electron Microscopy” (R. A. Steinbrecht and K. Zierold, eds.) pp. 175–191. Springer, Berlin.
- Müller-Reichert, T., Srayko, M., Hyman, A., O’Toole, E. T., and McDonald, K. (2007). Correlative light and electron microscopy of early *Caenorhabditis elegans* embryos in mitosis. *Meth. Cell Biol.* **79**, 101–119.
- Nanney, D. L. (1975). Patterns of basal body addition in ciliary rows in tetrahymena. *J. Cell Biol.* **65**, 503–512.
- Nozawa, Y. and Thompson, G. A., Jr. (1971). Studies of membrane formation in *tetrahymena pyriformis*. II. Isolation and lipid analysis of cell fractions. *J. Cell Biol.* **49**, 712–721.
- Orias, J. D., Hamilton, E. P., and Orias, E. (1983). A microtubule meshwork associated with gametic pronucleus transfer across a cell-cell junction. *Science* **222**, 182–184.
- O’Toole, E. T., Giddings, T. H.Jr., and Dutcher, S. K. (2007). Understanding microtubule organizing centers by comparing mutant and wild-type structures with electron tomography. *Meth. Cell Biol.* **79**, 125–143.
- O’Toole, E. T., Giddings, T. H., Jr., McIntosh, J. R., and Dutcher, S. K. (2003). Three dimensional organization of basal bodies from wild-type and delta-tubulin deletion strains of *Chlamydomonas reinhardtii*. *Mol. Biol. Cell* **14**, 2999–3012.
- Pearson, C. G., Giddings, T. H.Jr., and Winey, M. (2009a). Basal body components exhibit differential protein dynamics during nascent basal body assembly. *Mol. Biol. Cell* **20**, 904–914.
- Pearson, C. G., Osborne, D.P.S., Giddings, T. H., Jr., Beales, P. L., and Winey, M. (2009b). Basal body stability and ciliogenesis requires the conserved component poc1. *J. Cell Biol.* **187**, 905–920.
- Pearson, C. G., and Winey, M. (2009). Basal body assembly in ciliates: The power of numbers. *Traffic* **10**, 461–471.

- Sharma, N., Bryant, J., Wloga, D., Donaldson, R., Davis, R. C., Jerka-Dziadosz, M., and Gaertig, J. (2007). Katanin regulates dynamics of microtubules and biogenesis of motile cilia. *J. Cell Biol.* **178**, 1065–1079.
- Stemm-Wolf, A. J., Morgan, G., Giddings, T. H., Jr., White, E. A., Marchione, R., McDonald, H., and Winey, M. (2005). Basal body duplication and maintenance require one member of the *Tetrahymena thermophila* centrin gene family. *Mol. Biol. Cell* **16**, 3606–3619.
- Turkewitz, A. P., Orias, E., and Kapler, G. (2002). Functional genomics: The coming of age for *Tetrahymena thermophila*. *Trends Genet.* **18**, 35–40.
- Ueno, H., Gonda, K., Takeda, T., and Numata, O. (2003). Identification of elongation factor-1a as a Ca<sup>2+</sup>/calmodulin-binding protein in cilia. *Cell Motil. Cytoskeleton* **55**, 51–60.
- Yu, L. and Gorovsky, M. A. (2000). Protein tagging in *tetrahymena*. *Methods Cell Biol.* **62**, 549–559.